I&EC research
Industrial & Engineering Chemistry Research

Article

pubs.acs.org/IECR

Impinging Flame Characteristics in an Opposed Multiburner Gasifier

Yan Gong, Qinghua Guo, Jie Zhang, Puxing Fan, Qinfeng Liang, and Guangsuo Yu*

Key Laboratory of Coal Gasification and Energy Chemical Engineering of Ministry of Education, Shanghai Engineering Research Center of Coal Gasification, East China University of Science and Technology, Shanghai 200237, PR China

ABSTRACT: On the basis of the bench-scale opposed multiburner (OMB) gasifier, industrial light field camera and high speed cameras combined with high temperature endoscopes and image processing technology are proposed and applied to study characteristics of impinging flame height including impinging height and pulsation frequency in coal−water slurry (CWS) gasification. The results show that the mean flame height and the max flame height rise with the increase of mole ratio of oxygen to carbon (O/C) while the general increase trends decrease. The restriction of refractory dome to the flow field in impinging stream recirculation region enhance with the increase of O/C. The impinging flame heights calculated by light field camera combined with axial high temperature endoscope are proved to be reliable. Flame pulsation frequency is investigated by correlation coefficients and frequency spectra calculated from lateral high temperature endoscopes of 90° and 45° optical axis-to-target angle combined with high speed cameras. The characteristic frequency is below 10 Hz and variation ranges in correlation coefficients decrease while the stability of gasification enhances with the increase of O/C. The lateral imaging system of 90° optical axis-to-target angle clearly reflects the stability of gasification while the lateral imaging system of 45° optical axis-to-target angle could reflect the stability of impinging flames in burner plane.

1. INTRODUCTION

Coal gasification is a time-tested, reliable, and flexible technology that converts coal into a synthesis gas without burning it that then be used to produce chemical or other products.[1] Gasification technology has become a critical tool in the expansion of economy, allowing a wide variety of industrial products and fuels to be created from low-cost abundant coal resources especially in China.[2]

Developed during the 1990s, the opposed multiburner (OMB) gasification technology of East China University of Science and Technology (ECUST) with the capacity of 1150 t coal/day (4.0 MPa) was first demonstrated in 2005.[3] Since then, OMB gasification has been selected for over 30 projects that are either operating, under construction, or in the development phase.[4]

The flow field in the OMB gasifier has already been tested and reported.[5] As one of the key influencing factors of long operation period for gasification, the refractory wall would be probably impacted by high temperature (about 1800−2500 K)[6] flow erosion in impinging stream recirculation region and refraction-back stream region,[7] which will cause higher temperature during the later period of gasifier operation and replacement of partial refractory wall.[8] In order to provide a theory for predicting over temperature of the gasifier, the impinging flame behaviors including impinging flame height and pulsation frequency are investigated.

The height of diffusion flames are measured and estimated by researchers:[9] Thomas[10] defined the average flame height as the corresponding height where participating air and combustible gas completely react. On the basis of abundant experiments, both Zukoski[11] and Heskestad[12] obtained empirical formulas for estimating flame height. For jet diffusion flames, Mikofski[13] measured the height of laminar inverse diffusion flame based on planar laser-induced fluorescence (PLIF) and compared to the results and analysis that Roper[14] had made for normal diffusion flames. Kiran[15] measured the lift-off height and flame length for a simple LPG (liquefied petroleum gas) jet diffusion flames. On the basis of experiments and numerical calculations, Chuah[16] added vortex flows around Burke−Schumann diffusion flames to predict the flame heights and the flame shapes of small fire whirls. Since the feature of flames in OMB gasifier differ from normal diffusion flames, specific measurements are carried out.

The bench-scale OMB gasifier is operated under high temperature with positive pressure, and refractory wall is wrapped by ceramic fiber blanket inside the stainless steel shell. As a result, the view to the internal gasifier is greatly limited. In order to obtain reliable three-dimensional (3D) structural information of impinging flames in gasifier based on a single view, industrial light field camera is applied.

The concept of light field camera, also called plenoptic camera, was first proposed by Gabriel Lippmann in 1908,[17] and it is able to capture the 2D photograph of the total amount of light at each point on the camera sensor as well as the full 4D light field measuring the amount of light traveling along each ray that intersects the sensor in a single photographic exposure.[18] With developments in theory, Adelson[19] proposed the design of a light field camera that can be used to significantly reduce the correspondence problem in stereo matching. Since then, diverse kinds of light field camera had been designed and manufactured.[20,21] Ng[22] presented hand-held light field camera where a micro lens array is placed in front of the image sensor that samples the 4D light field information in 2005 and demonstrated commercial light field cameras in 2011 that targeted to consumer use. The first commercially available industrial light field camera was produced by the company Raytrix with an increased effective spatial resolution, an extended depth of field and algorithms for

Received: October 12, 2012
Revised: January 16, 2013
Accepted: January 25, 2013
Published: January 25, 2013

dx.doi.org/10.1021/ie3027857 | Ind. Eng. Chem. Res. 2013, 52, 3007−3018

refocusing, view manipulation, and scene depth calculation which focuses on industrial and scientific applications,.

The coal−water slurry (CWS) flames in OMB gasifier are severely impinged and pulse axially, although the feature of flame height in the gasifier is different from that of diffusion flames, the method of analysis could be carried out in the same way. On the basis of the bench-scale OMB gasifier, the impinging flames of CWS are visualized by industrial high speed camera, light field camera, and high temperature endoscope. The relationship between operating condition and flame characteristics including impinging flame height and pulsation frequency is discussed in order to provide theoretical foundations for the optimal design and operation of industrial OMB gasifier.

2. MEASUREMENT PRINCIPLES

2.1. Light Field Camera. The schematic of a light field camera is shown in Figure 1.

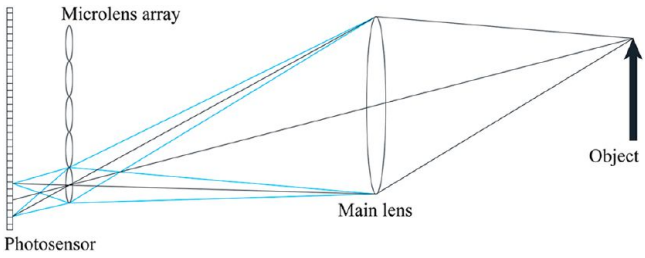

Figure 1. Schematic of a light field camera.

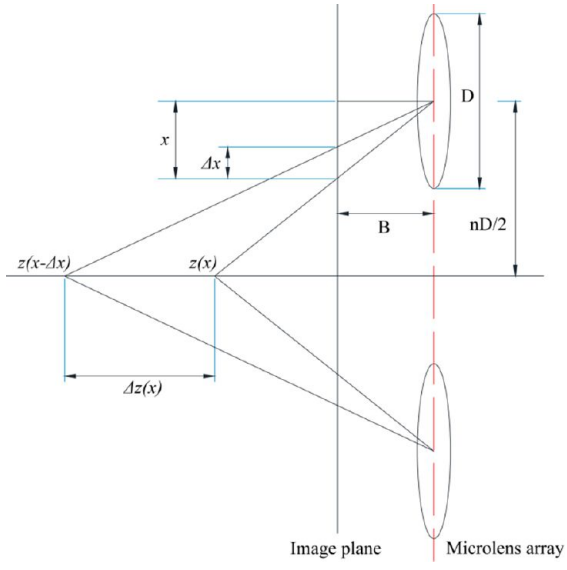

Figure 2. Geometric construction for depth estimation.

The light field camera consists of a main lens and an array of microlenses installed close to the photosensor. Rays of light from a single point on the subject are brought to a single convergence point on the focal plane of the microlens array and these rays of light are separated by the microlens based on direction, generating a focused image of the aperture of the main lens on the array of pixels on photosensor behind the microlens. The light field camera captures multiple views of a scene in a single snapshot, which samples the light field providing angular as well as spatial information on the

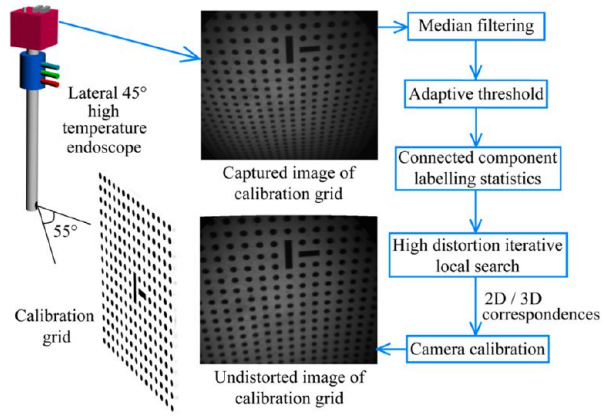

Figure 3. Algorithm of distortion correction.

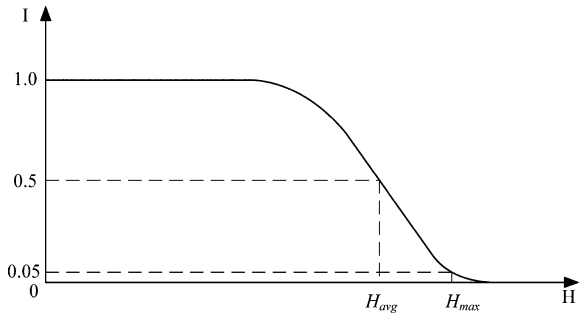

Figure 4. Definition of mean flame height and max flame height.

distribution of light rays in space.[22] As the depth of the recorded scene could be estimated from a single raw image of light field camera, reconstructing the 3D surfaces of objects in the scene becomes an important industrial application besides the digital refocusing.[23]

Bishop[24] proposed an alternative iterative approach to depth estimation. The depth resolution varies on the position of a line parallel to the optical axes and lying half way between two micro lenses. Figure 2 shows the geometric construction for depth estimation.

The line which connects the center of a microlens and a single point in the image plane that distance x from the center of the micro-image intersects the central bisecting line at $z(x)$. Define Δx as the size of a pixel, and the line connects the image point at the adjoining pixel and the center of the micro lens mentioned above intersects the central bisecting line at $z(x - \Delta x)$. Thus the distance between $z(x)$and $z(x - \Delta x)$ is regarded as the depth resolution for a pixel at distance x from the center of the micro-image, and the relation between z and x is given by

$$z = \frac{nDB}{2}/x, \qquad n = 1, 2, ..., N \tag{1}$$

The point at distance $z(x)$ from the micro-image plane can be projected back through the main lens into the corresponding object space using the thin lens equation:

$$\frac{1}{f} = \frac{1}{o} + \frac{1}{i} \tag{2}$$

where f refers to focal length, and the image distance i along the optical axis to which an object at distance o from the lens plane is projected, could be calculated by eq 2.

dx.doi.org/10.1021/ie3027857 | Ind. Eng. Chem. Res. 2013, 52, 3007−3018

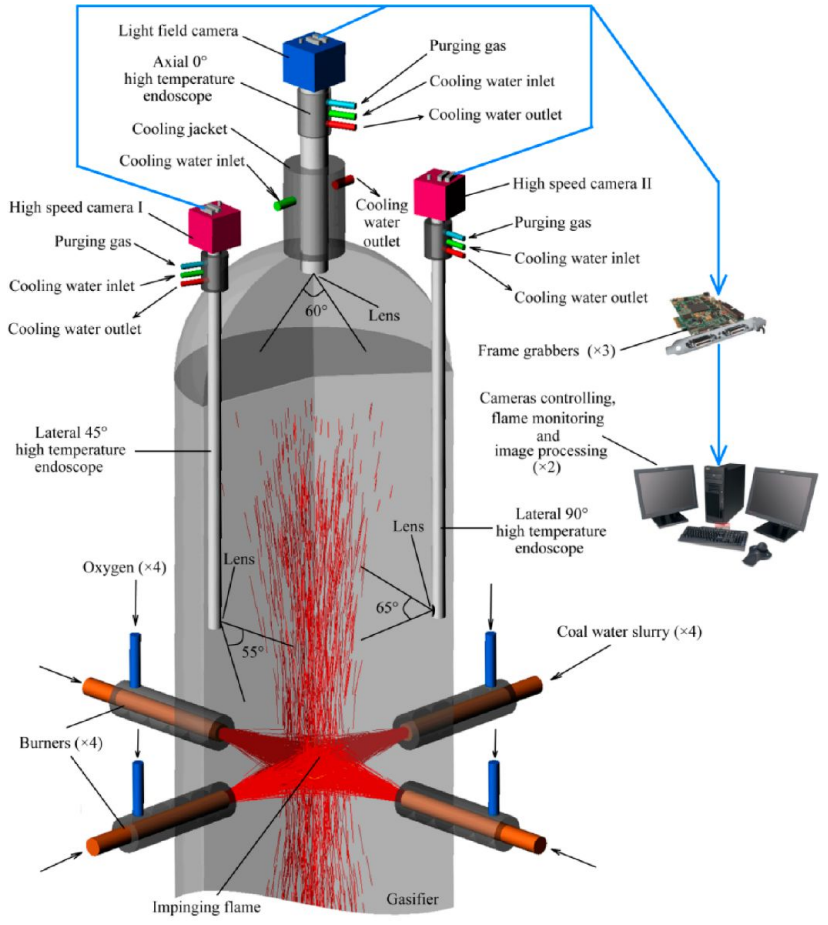

Figure 5. Schematic of the bench-scale OMB gasifier.

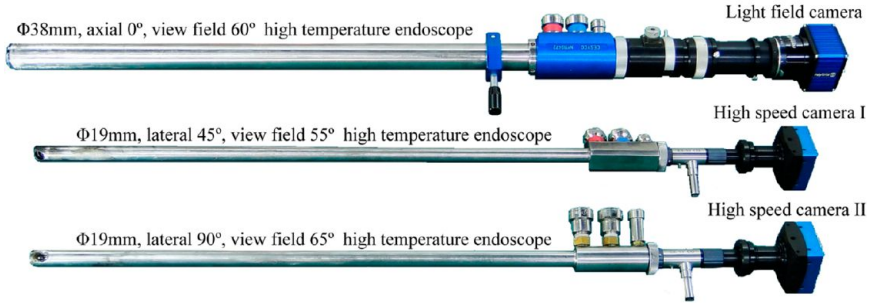

Figure 6. Combinations of industrial cameras and high temperature endoscopes.

The total covering plane is defined as the plane closest to the micro lens plane where each point on the plane is projected by at least one microlens, and z_0 denotes the distance of the total covering plane from the micro lensplane. Assume that the optimal focus plane of the main lens with a focal length of f_L locates at the plane z_0, and the distance between the main lens plane and the total covering plane at z_0 is defined as i_0. Thus, the depth positions in object space can be calculated by eq 3

$$o(x) = \left(\frac{1}{f_L} - \frac{1}{i_0 + z(x) - z_0} \right)^{-1} \tag{3}$$

Once the depth map is estimated, the 3D surface of a object in scene, such as the 3D structure of flames in gasifier, can be obtained.

2.2. Distortion Correction. High temperature endoscopes with wide-angle lens are applied for the purpose of acquiring larger field of view for flame in gasifier. As a result, geometric barrel distortion becomes a major influence for the measurement of flame height. Smith[25] and Hideaki[26] developed methods for endoscope distortion corrections, and Rottier[27] designed and manufactured a high temperature endoscope for endoscopic particle image velocimetry (PIV) system adapted to high temperature furnaces, of which the geometric barrel distortion is corrected. A calibration method for endoscope and other imaging systems developed by Wengert[28] is applied using the camera model of Heikkila.[29] A typical calibration procedure based on lateral high temperature endoscope of 45° optical axis-to-target angle is shown in Figure 3.

dx.doi.org/10.1021/ie3027857 | Ind. Eng. Chem. Res. 2013, 52, 3007−3018

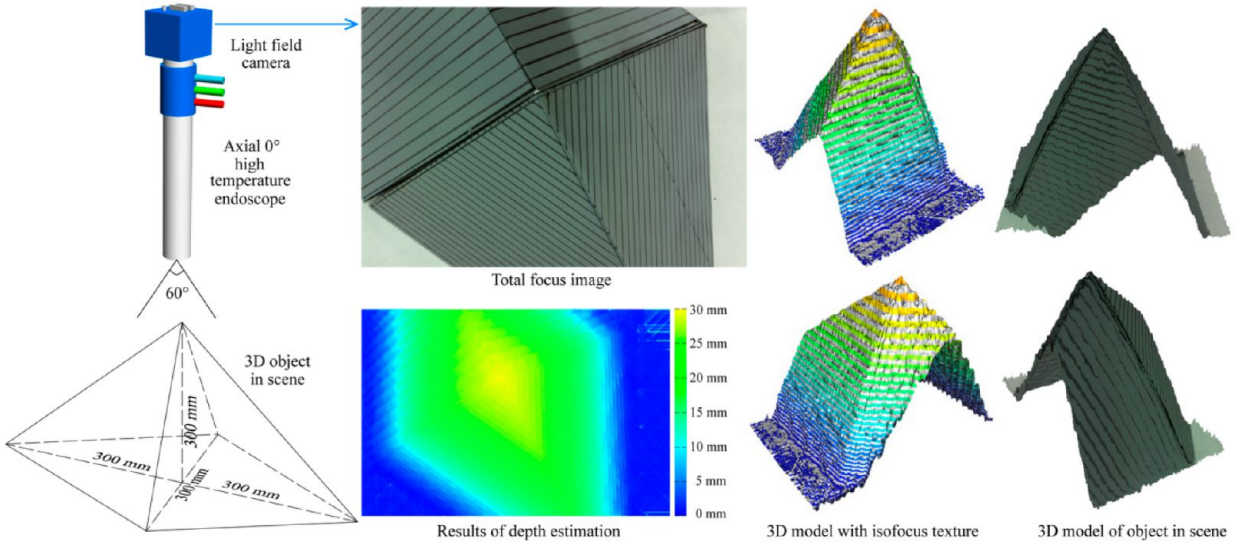

Figure 7. Depth estimation and reconstruction of the 3D object in scene.

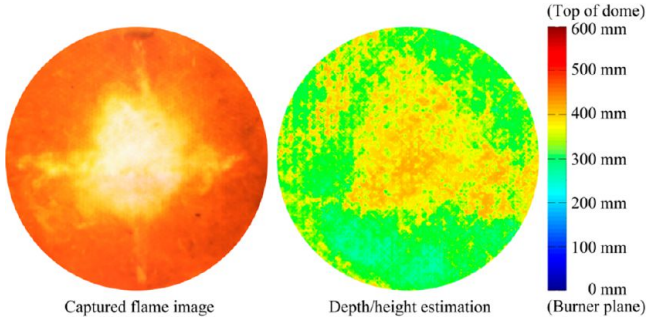

Figure 8. Depth/height estimation for a single image of impinging flame captured by light field camera combined with high temperature endoscope.

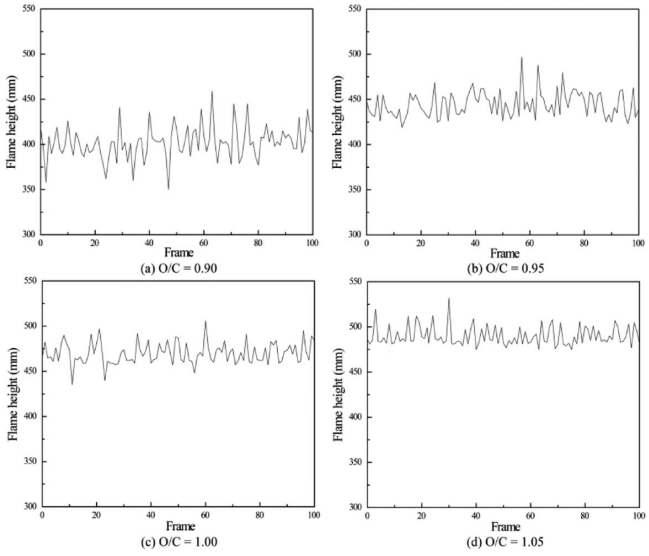

Figure 9. Impinging flame heights calculated by light field camera under different O/Cs.

First, at least 2 images (15 images are recommended) of the calibration grid should be taken from different viewpoints without additional or assistant illumination. After denoising the image with a 3 × 3-median filter, a low-pass filter is used to determine a local threshold for each pixel. From the binary image, all blobs are extracted using connected component labeling and each blob is characterized with statistical and geometric properties. Then the two special marks are recognized and the orientation of them gives two directions to start searching for adjacent points, and the image coordinates could be used to calculate a projective transformation between the points and their grid coordinates. The final projective transformation between all matched point pairs would be computed when all correspondences are found. Finally, the camera's intrinsic parameters are obtained and the geometric barrel distortion of an endoscopic image could be corrected.

2.3. Definition of Flame Height. In order to provide reliable definition for pulsating flames in gasifier, the mean flame height and max flame height are defined. The luminosity of the lower part of the flaming region appears steadier than that of the intermittent upper part. The graph in Figure 4 is generally used to define the flame height.[11]

The intermittency, denoted I, is shown on the longitudinal ordinate, where a value of 1 indicates the appearance of a flame at all times. The horizontal ordinate shows the distance above the burner plane in gasifier, H. The flame height at which the intermittency is 0.5, i.e., the height above which flame appears half the time, is defined as the mean flame height, H_{avg}. The flame height at the intermittency of 0.05 is defined as the max flame height, H_{max}, which is a particular parameter for the analysis of predicting over temperature for gasifier.

2.4. Flame Pulsation Frequency. As an important characteristic of impinging flame, pulsation of flame could be characterized by pulsation frequency. Since the pulsation of flame could greatly affect the gasificating speed, flame height, combustion efficiency, and flame structure, many researchers have concluded prediction models and empirical formulas for estimating flame pulsation frequency for various kinds of flame based on abundant experiments.[30−33]

Since the strong visible radiation generated from refractory wall at high temperature causes great background disturbance to the illumination of impinging flames, traditional ways would not be suitable for the measurement of flame pulsation frequency. A new method for analyzing the flame pulsation frequency is provided by applying fast Fourier transform to

dx.doi.org/10.1021/ie3027857 | Ind. Eng. Chem. Res. 2013, 52, 3007−3018

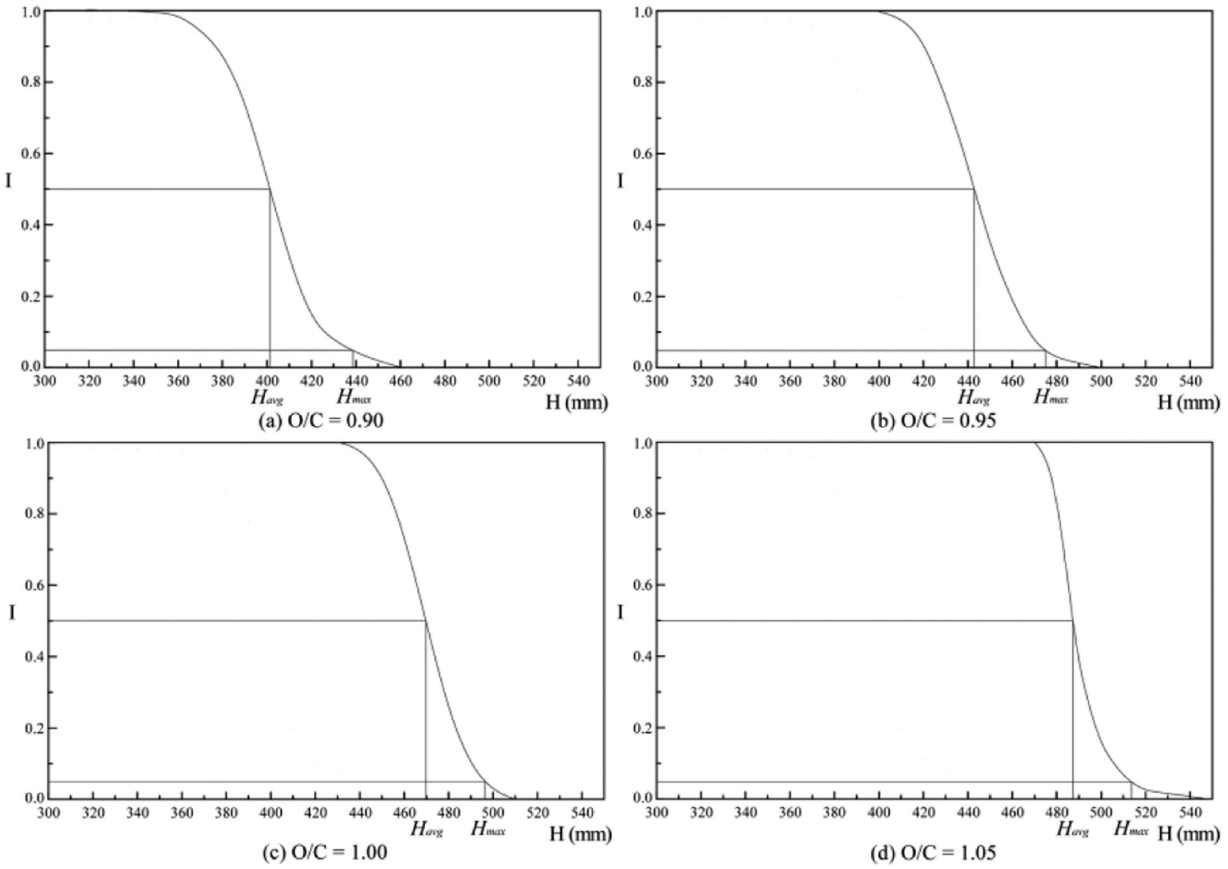

Figure 10. Intermittencies of impinging flame heights under different O/Cs based on light field camera.

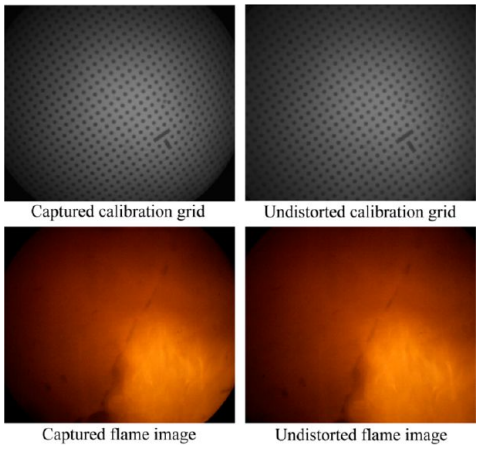

Figure 11. Distortion correction of lateral 90° imaging system.

time variation of image correlation coefficients of sequence images.[34] In order to reduce the error in calculation, a average image of 10 continuous images is selected as the reference image. Each flame image in sequence is compared to the reference image and a sequence of correlation coefficients is generated. The mean dual scale edge structure similarity (MDESSIM) method[35] is used in the process of correlation analysis of two images, by which the correlation coefficient of the reference image and an individual image in sequence could be calculated quantitatively and objectively. The luminosity comparison function, the contrast comparison function, and the structural character similarity of macro-edges combined with micro-edges comparison function are integrated in the MDESSIM evaluation method. The value of correlation coefficient varies from 0 to 1, and a great change between two continuous correlation coefficients indicates a severe instantaneous pulsation of flame.

Flame pulsation frequency presents a unique characteristic in OMB gasifier compared to that of normal diffusion flames due to the specific internal structure and the feature of four opposed burners as well as the effect of high temperature, flow field, and synthesis gas composition. However, the fast Fourier transform

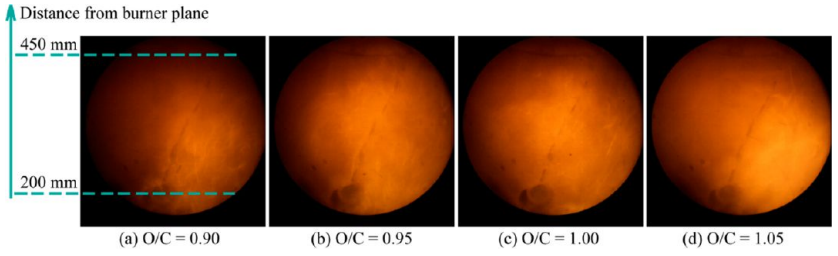

Figure 12. Impinging flame images captured by lateral 90° imaging system under different O/Cs.

dx.doi.org/10.1021/ie3027857 | *Ind. Eng. Chem. Res.* 2013, 52, 3007−3018

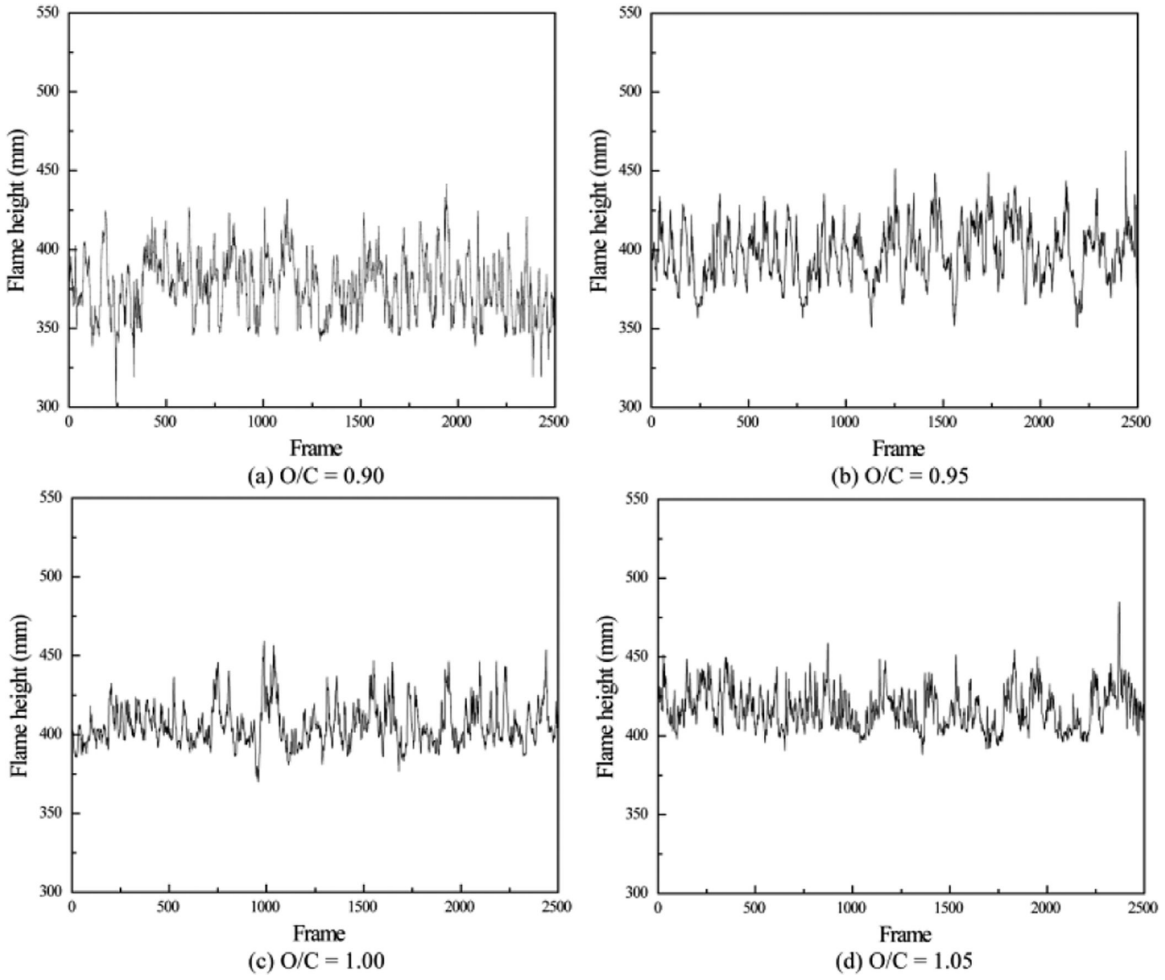

Figure 13. Impinging flame heights measured by lateral 90° imaging system under different O/Cs.

(FFT) to time variation of image correlation coefficients is still appropriate for flame pulsation frequency analysis.

3. EXPERIMENTAL SETUP

The diagram of the bench-scale OMB gasifier is shown in Figure 5. The four nonpremixed burners are side mounted oppositely in a horizontal plane with the angle of 90° between each other. Diesel is introduced during the preheating procedure. When the interior temperature of gasifier reaches 1473 K, CWS is injected into the gasifier through the center of two-channel burners by monopumps and atomized by high velocity oxygen transported through annulus which supplied by liquid oxygen in dewar vessels. In the gasification chamber, four mixed streams of CWS and oxygen react under reducing conditions to produce raw syngas.

The inner diameter of the refractory wall in gasifier is 300 mm, and the distance from burner plane to the top of dome is 600 mm with the ratio of height to diameter of 2.0. The CWS made of Shenfu coal with solid content of 61% is gasified at positive pressure, and the average flow rate remains at 11.50 kg/h along with the oxygen flow rate varying from 5.70 N to 6.90 N m^3/h for each burner, which is controlled and measured by gas mass flow meters in order to change the mole ratio of oxygen to carbon (O/C) at 0.90, 0.95, 1.00, and 1.05, respectively.

The impinging flame in the gasifier is visualized by three sets of imaging systems as shown in Figure 6. A CESYCO Φ38 mm axial high temperature endoscope of 0° optical axis-to-target angle with 60° view field (axial 0° high temperature endoscope) combined with a Raytrix R29 industrial light field camera is installed on the top of refractory wall and cooperated with a frame grabber, a graphics workstation, and associated image processing software in order to obtain 2D and 3D information of impinging flames in an axial direction. A CESYCO Φ19 mm lateral high temperature endoscope of 45° optical axis-to-target angle with 55° view field (lateral 45° high temperature endoscope) and the other CESYCO Φ19 mm lateral high temperature endoscope of 90° optical axis-to-target angle with 65° view field (lateral 90° high temperature endoscope) which combined with Mikrotron MC1363 industrial high speed cameras are laterally installed in order to directly obtain the impinging flame images in radial directions at different heights by moving the endoscopes up or down. Each imaging system runs with water cooling and inert gas purging to avoid excessive heat and keep lenses clean.

Since the resolution of correspondence between lateral 45° high temperature endoscope and length/height graduated scale is much lower in far field of view during the calibration procedure which could not meet the requirement for flame height measurement, only the light field camera and lateral 90° imaging system are used to calculate and measure the impinging flame height in different ways in order to choose an optimal method for industrial application.

It is not appropriate to calculate the flame pulsation frequency from flame images captured by R29 light field

dx.doi.org/10.1021/ie3027857 | Ind. Eng. Chem. Res. 2013, 52, 3007−3018

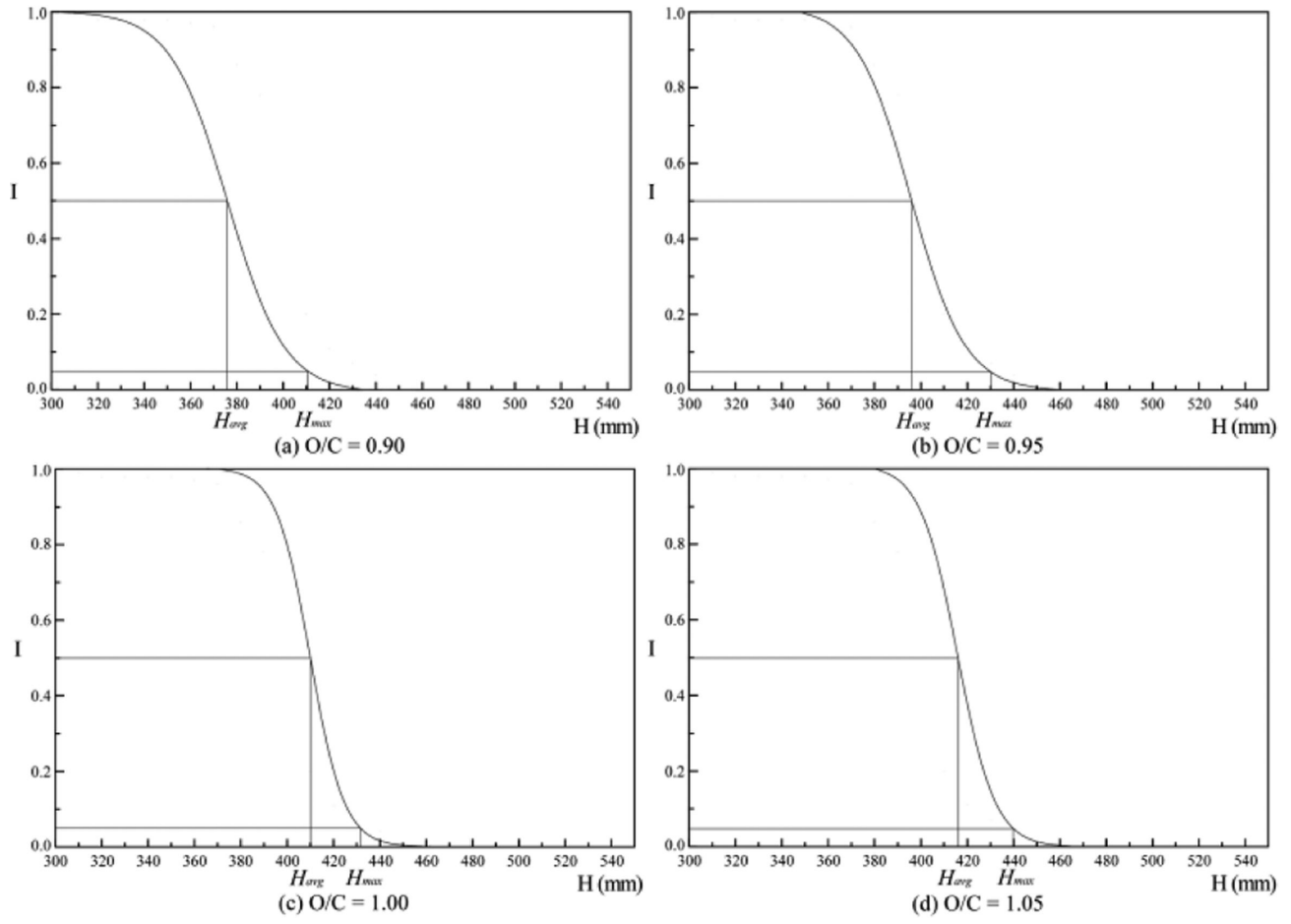

Figure 14. Intermittencies of impinging flame heights under different O/Cs based on lateral 90° imaging system.

Table 1. Results of Average Flame Height and Max Flame Height

	results calculated by light field camera		results measured by lateral imaging system	
O/C	H_{avg}/mm	H_{max}/mm	H_{avg}/mm	H_{max}/mm
0.90	402	438	376	411
0.95	443	475	396	430
1.00	470	496	410	432
1.05	487	514	417	439
$H_{(O/C=1.05)} - H_{(O/C=0.90)}$	85	76	41	28

camera since the max frame rate is limited to 6 fps which could not meet the requirement of sampling frequency of impinging flames. As a result, flame pulsation frequency in gasifier is measured by lateral 90° imaging system and lateral 45° imaging system respectively, and the results are compared with each other to analyze the pulsation frequency of impinging flames in different regions of gasifier.

4. RESULTS AND ANALYSIS

4.1. Impinging Flame Height. *4.1.1. Height Calculation with Light Field Camera.* Before the customized R29 industrial light field camera is applied in gasifier, the algorithm for depth estimation has to be verified and calibrated.

A 3D object is captured by the light field camera as shown in Figure 7. With a single photographic exposure, every focusable plane is in focus and a total focus image is calculated by accompanied software and workstation. As the object is marked with standard contour lines, the depth map of the 3D object surface in scene is estimated and calibrated. In this way, the 3D model of the object is reconstructed. The results show that the algorithm for quantitative depth estimation is feasible and reliable.

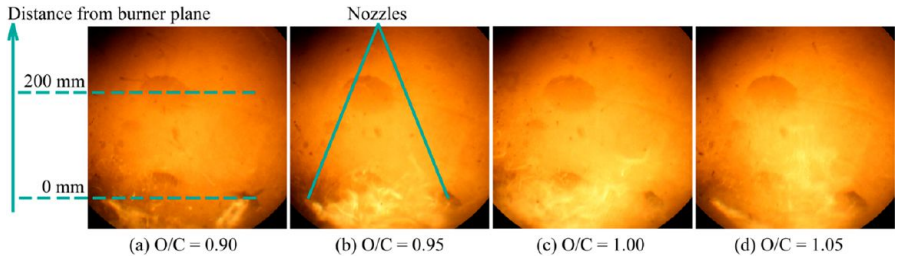

Figure 15. Impinging flame images captured by lateral 45° imaging system under different O/Cs.

dx.doi.org/10.1021/ie3027857 | Ind. Eng. Chem. Res. 2013, 52, 3007−3018

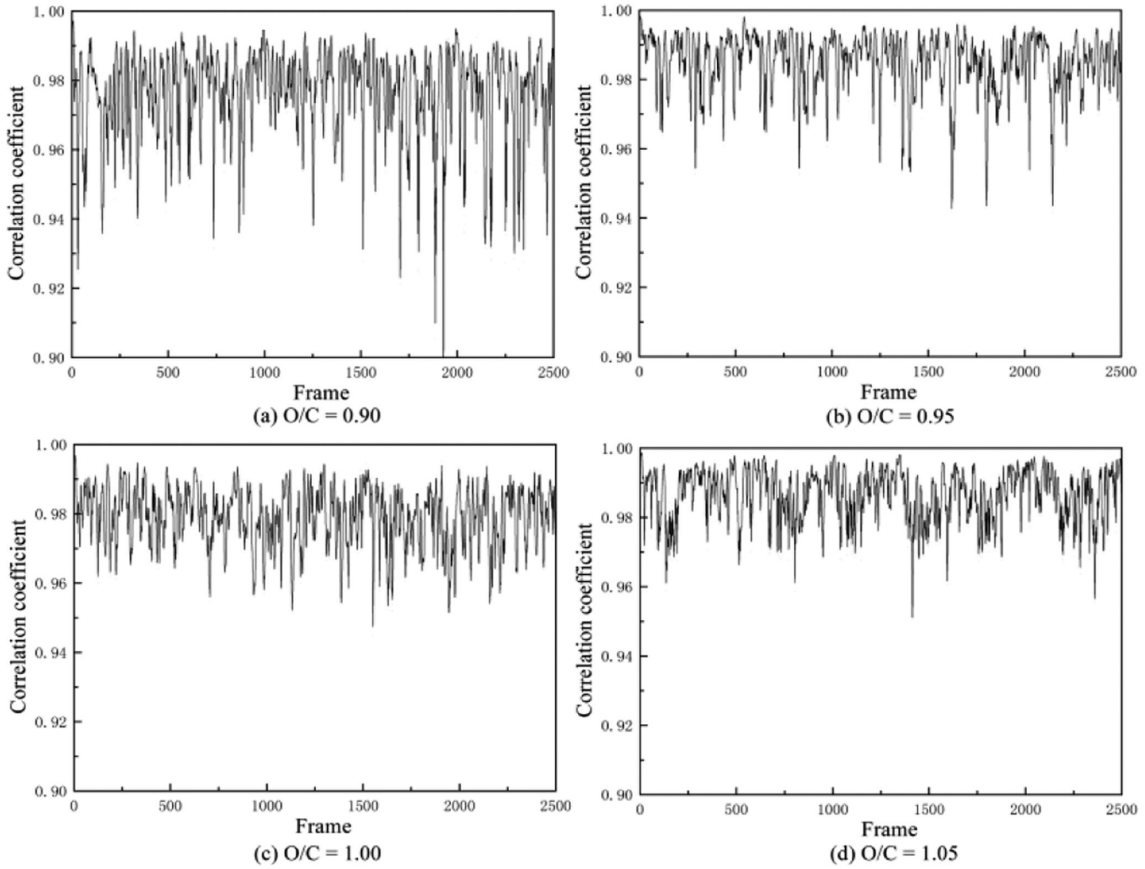

Figure 16. Correlation coefficients under different O/Cs for lateral 90° imaging system.

On the basis of the bench-scale OMB gasifier, CWS is gasified under the operating conditions mentioned in section 3. The flame images are captured at the speed of 6 fps in the axial direction by Φ38 mm high temperature endoscope combined with the customized light field camera at different mole ratio of oxygen to carbon (O/C) of 0.90, 0.95, 1.00, and 1.05.

Figure 8 shows typical depth/height estimation for the impinging flame. The four flame torches form a cross flame structure and the impinged flame extends in axial directions. The max flame height in Figure 8 could reach about 500 mm, and a flame deviation from the axis can be observed obviously. Each of the sequence flame images is processed in order to calculate the 3D information of impinging flames; in this way the flame heights in the axial direction at different operating conditions are obtained as shown in Figure 9, based on which the intermittencies are calculated as shown in Figure 10.

4.1.2. Height Measurement with High Speed Camera. The results calculated from light field camera can be compared with that from the set of Φ19 mm lateral high temperature endoscope combined with industrial high speed camera. Flame images under different operating conditions are captured in order to obtain the impinging flame heights laterally. The calibration grid developed by Wengert[28] is applied to the imaging system, and the flames images are undistorted based on calibration parameters.

The undistorted images from lateral 90° imaging system are shown in Figure 11. All of the flame images in sequence captured by the imaging system are corrected and corresponded to length/height graduated scale in pixels, through which the exact impinging flame heights could be obtained. Since the resolution of correspondence between lateral 45° high temperature endoscope and length/height graduated scale is much lower in far field of view which could not meet the requirement for flame height measurement, only the lateral 90° high temperature endoscope is applied.

Flame images are captured by high speed cameras at the speed of 250 fps for 10 s under different O/Cs of 0.90, 0.95, 1.00, and 1.05. Typical impinging flame images are shown in Figure 12. The flame temperature is about 1900 K while the temperature of refractory wall could reach around 1400 K. As a background disturbance, the refractory wall generates strong visible radiation compared to the chemiluminescence and soot radiation from flame. Therefore, image processing of gray scale, image denosing, and threshold segmentation are applied to the flame images after distortion correction, and the impinging flame heights that vary with time are obtained as shown in Figure 13, based on which the intermittencies are calculated as shown in Figure 14.

4.1.3. Results and Analysis of Impinging Flame Height. The results of impinging flame height obtained from two methods show that both the mean flame height H_{avg} and the max flame height H_{max} rise with the increase of O/C while the general increase trends decrease, the variation ranges also reduce. The rise of H_{avg} in height is higher than that of H_{max} with the increase of O/C as shown in Table 1.

Within the operating conditions in O/C, the rise of H_{avg} in height is higher than that of H_{max} with the increase of O/C which reflects that the restriction of refractory dome to the flow field in impinging stream recirculation region is enhanced. The variation ranges in H_{avg} and H_{max} calculated by light field camera are wider than the results measured by lateral 90° imaging system. Correspondingly, the values of impinging

dx.doi.org/10.1021/ie3027857 | Ind. Eng. Chem. Res. 2013, 52, 3007−3018

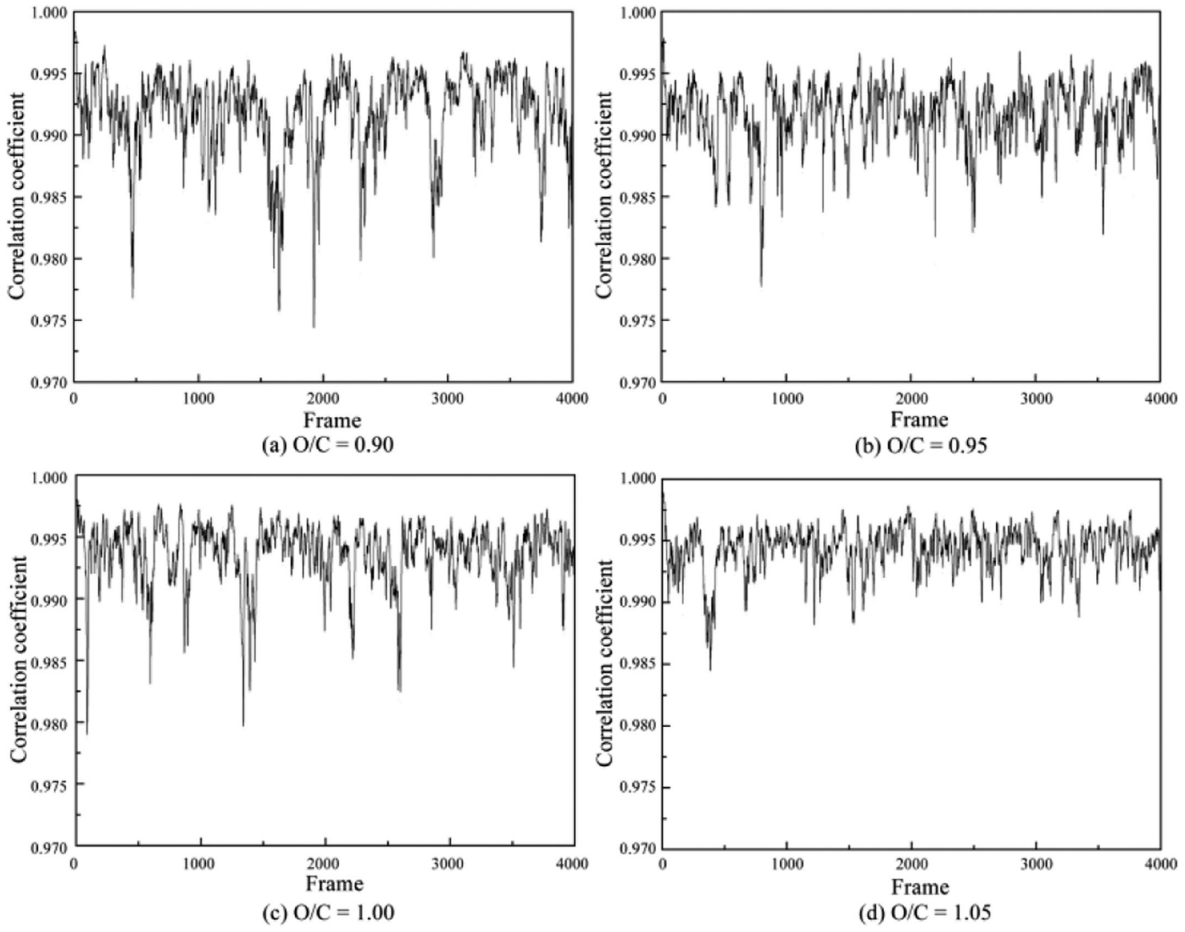

Figure 17. Correlation coefficients under different O/Cs for lateral 45° imaging system.

flame height calculated by light field camera are higher than the results from the lateral 90° imaging system at same O/Cs.

The main reason for the differences in results between the two methods is the limitation in view angle of the lateral 90° high temperature endoscope and inner diameter of the refractory wall. The impinging flame pulsates in axial direction, since it could possibly exceed the view of field of the endoscope, while the vignette in the perimeter of flame images could affect the judgment on flame edges. These effects could decrease the measured impinging flame height together. The flame deviation from axis is observed in the bench-scale OMB gasifier since the small size of bench-scale gasifier could cause certain errors in machining which may not appear in large-scale industrial gasifier, and this phenomenon could not be visualized by the lateral 90° imaging system which would also affect the measured results of flame height. The flame deviation from axis after impinged is mainly caused by the machining errors of the small size nozzles which results in deflection of flame torches Since the direction and magnitude of deviation from axis are steady and small respectively, the effect on results of flame height is limited.

As the illumination of impinging flame is closely associated with the flame temperature, the temperature distribution could directly reflect the impinging flame height in gasifier. Comparing the impinging flame heights calculated by light field camera and measured by lateral 90° imaging system to the measured flame temperature data and reconstructed 3D temperature distribution in OMB gasifier,[6] the increase of impinging flame height agree well with the rise of high temperature region in axial direction with the increase of O/C. Therefore, the impinging flame heights calculated by light field camera show a better regularity than that from lateral 90° imaging system and the light field camera is proved to be reliable in calculation of impinging flame height.

According to the impinging flame height calculated by light field camera, the max flame height H_{max} is above 450 mm which refers to the joint plane of dome and cylinder refractory wall at the O/C between 0.95 and 1.05, the mean flame height H_{avg} would also exceed the joint plane at the O/C of 1.00 and 1.05. When the impinging flame exceeds to the dome of gasifier, it could occasionally eroded the refractory wall in dome. During the operation of bench-scale OMB gasifier, the flame deviation from axis is observed, and this phenomenon could be aggravated by the nozzle wear during long period operation, which will affect the flow field in gasifier and aggravate the erosion to dome refractory wall and lead to over temperature in dome. As a result, the average ratio of impinging flame height to diameter is limited to 1.48 when the operating condition of O/C is controlled between 0.90 and 0.95 for the OMB gasifier with the ratio of height to diameter of 2.0.

4.2. Flame Pulsation Frequency. It is not appropriate to calculate the flame pulsation frequency from flame images captured by R29 light field camera since the max frame rate is limited to 6 fps while the characteristic pulsation frequency of impinging flames in gasifier could be more than 6 Hz. Therefore, high speed cameras combined with lateral high temperature endoscopes are applied to capture sequence flame images. Typical flame images captured by lateral 90° and 45° imaging systems under different C/Os are shown in Figures 12 and 15, respectively.

dx.doi.org/10.1021/ie3027857 | Ind. Eng. Chem. Res. 2013, 52, 3007−3018

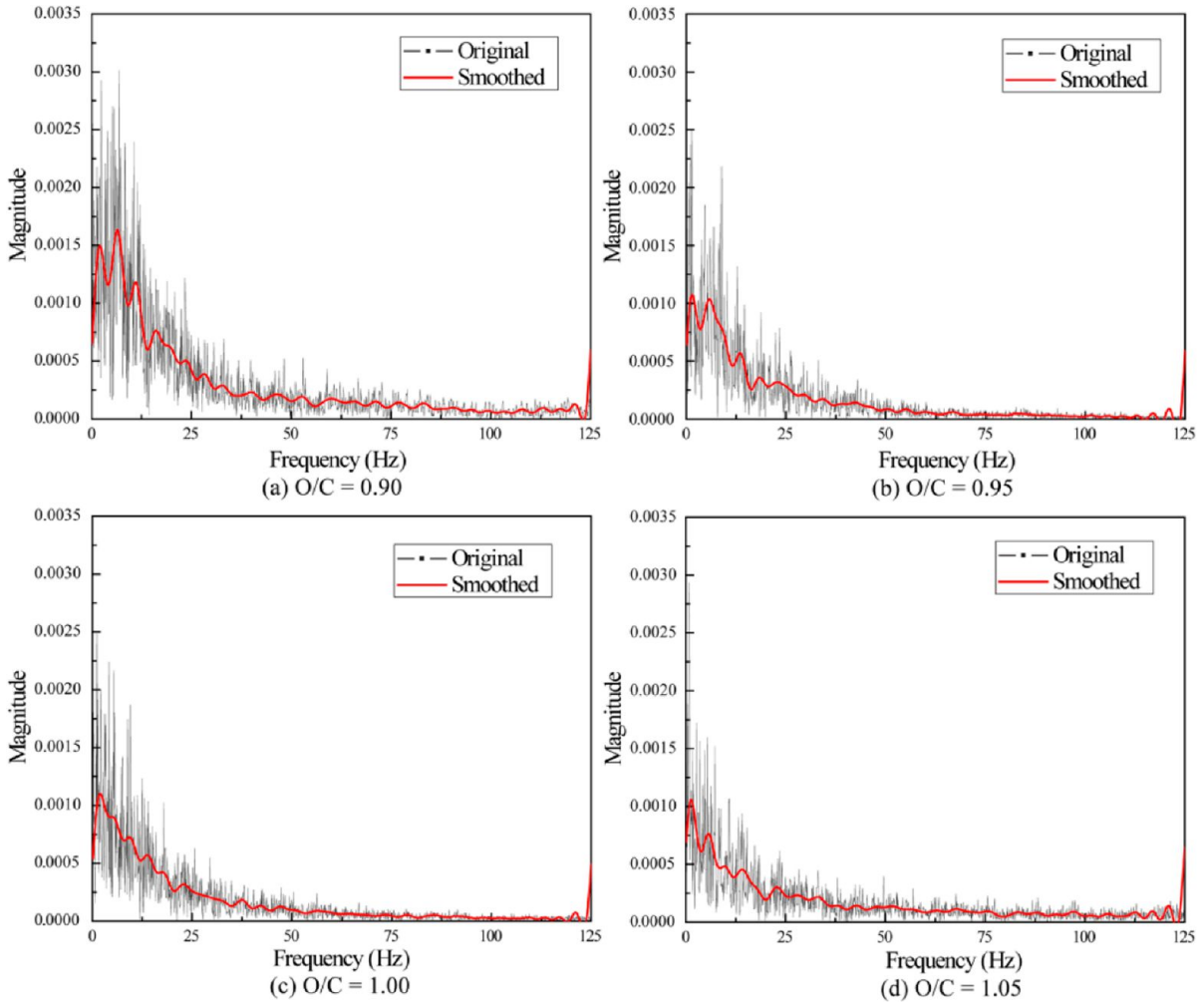

Figure 18. Frequency spectra under different O/Cs for lateral 90° imaging system.

An average image of 10 continuous images is selected as the reference image, while the MDESSIM method is applied to calculate correlation coefficient for each image in sequence. The correlation coefficients of images captured from lateral 90° imaging system (250 fps, 10 s) and 45° imaging system (600 fps, 6.67 s) under different O/Cs of 0.90, 0.95, 1.00, and 1.05 are shown in Figures 16 and 17, respectively.

The variation ranges of correlation coefficients calculated from lateral 45° imaging system is much smaller than that of lateral 90° imaging system. As a result, the longitudinal ordinate range of the results from lateral 45° imaging system is relatively smaller in order to analyze correlation coefficients with detailed data.

Then, the frequency spectra are calculated by the FFT of correlation coefficients as shown in Figures 18 and 19, respectively. Correspondingly, the range of magnitude in longitudinal ordinate of the results from lateral 45° imaging system is relatively smaller for observing details.

As the curves of frequency spectra under different O/Cs have high-frequency noise, the FFT filtering method is applied to smooth the data. FFT filter smoothing is accomplished by removing Fourier components with frequencies higher than a cutoff frequency of

$$F_{\text{cutoff}} = 1/n_{\text{dp}}\Delta t_{\text{dp}} \tag{4}$$

where n_{dp} is the number of data points and Δt_{dp} is the time spacing between two adjacent data points. According to the sampling parameters, the cutoff frequencies are 0.1 and 0.15 Hz for a lateral 90° imaging system and lateral 45° imaging system, respectively. Thus high-frequency noise is removed and the red curves represent smoothed data of magnitude in Figures 18 and 19.

According to the results of correlation coefficients and frequency spectra calculated from lateral 90° and lateral 45° imaging system, variation ranges in correlation coefficients decrease with the increase of O/C. The higher the average value of correlation coefficient, the smaller the difference between each flame image and the reference image, which indicates the stability of gasification enhances with the increase of O/C. The characteristic frequency is below 10 Hz, the characteristic frequency and the corresponding magnitude decrease with the increase of O/C, and the stability of flame enhances to a stable degree at the O/C of 1.00. The results from two imaging system agree well with each other.

The correlation coefficients calculated from lateral 45° imaging system at different O/Cs is higher than that from lateral 90° imaging system, which is mainly caused by the view of field in lateral 45° imaging system that covers most of the impinging flame and part of flame torches, including the steady lower region of the impinging flame. The magnitude in frequency spectra calculated from lateral 90° imaging system is much higher than that from lateral 45° imaging system and the characteristic peaks decrease faster with the increase of O/C in frequency spectra calculated from lateral 90° imaging system, which reflect that stability of impinging flame enhances with the

dx.doi.org/10.1021/ie3027857 | Ind. Eng. Chem. Res. 2013, 52, 3007−3018

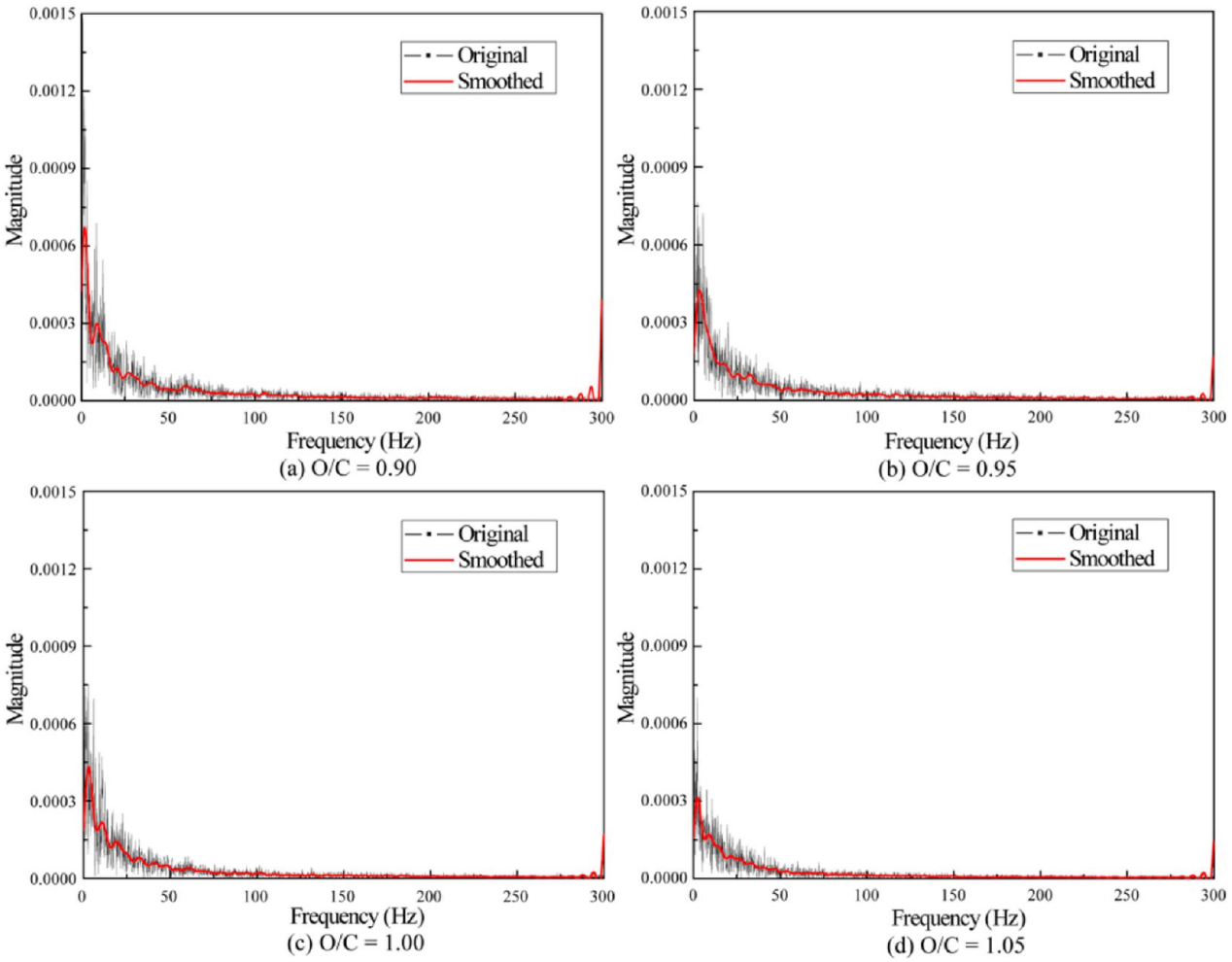

Figure 19. Frequency spectra under different O/Cs for lateral 45° imaging system.

increase of O/C and indicates that the lateral 90° imaging system is more sensitive to the stability of gasification in upper region of gasifier. Distinct characteristic peaks below 3 Hz decrease with the increase of O/C in frequency spectrum which is observed from lateral 45° imaging system and the variation of the characteristic peak is probably caused by the pulsation of flame torches in the burner plane. This regularity could be observed especially when looking into sequence images captured by high speed cameras. It can be perceived that the lateral 45° imaging system could reflect the stability of impinging flames in burner plane to a certain extent.

5. CONCLUSIONS

The impinging flame in the gasifier pulsates in the axial direction, and the variation ranges decrease with the increase of O/C. The results of impinging flame height calculated by a light field camera and measured by lateral 90° imaging system jointly show that both the mean flame height H_{avg} and the max flame height H_{max} rise with the increase of O/C while the general increase trends decrease, and the variation ranges also reduce. The rise of H_{avg} in axis is higher than that of H_{max} with the increase of O/C, which reflects that the restriction of refractory dome to the flow field in impinging stream recirculation region is enhanced. Comparing the impinging flame heights calculated by light field camera to the results measured by lateral 90° imaging system, the results from light field camera are proved to be reliable.

According to the results of correlation coefficients and frequency spectra calculated from lateral 90° and lateral 45° imaging system, the characteristic frequency is below 10 Hz and variation ranges in correlation coefficients decrease with the increase of O/C. The stability of gasification enhances with the increase of O/C and the stability enhances to a stable degree at the O/C of 1.00. The characteristic of flame pulsation frequency in upper region of impinging flame obtained from lateral 90° imaging system could clearly reflect stability of gasification while the lateral 45° imaging system could reflect the stability of impinging flames in burner plane to a certain extent.

According to the impinging flame height calculated by light field camera, the max flame height H_{max} is above 450 mm at the O/C between 0.95 and 1.05, the mean flame height H_{avg} would also exceed 450 mm at the O/C of 1.00 and 1.05. As a result, the average ratio of impinging flame height to diameter is limited to 1.48 when the operating condition of O/C is controlled between 0.90 and 0.95 for the OMB gasifier with the ratio of height to diameter of 2.0.

AUTHOR INFORMATION

Corresponding Author

*Tel: +86-21-64252974. Fax: +86-21-64251312. E-mail address: gsyu@ecust.edu.cn.

Notes

The authors declare no competing financial interest.

■ ACKNOWLEDGMENTS

This work is financially supported by the National Nature Science Foundation of China (21176078) and the National Key State Basic Research Development Program of China (973Program, 2010CB227004).

■ REFERENCES

(1) Gasification, An Investment in our Energy Future, Gasification Technologies Council Report. www.gasification.org (accessed 2012/9/24), 2011.
(2) Cheung, K. *Integration of Renewables, Status and Challenges in China*. International Energy Agency: Paris, 2011; working paper.
(3) Higman, C.; Burgt, M. *Gasification*; Gulf Professional Publishing: Oxford, U.K., 2008.
(4) Ondrey, G. Coal to Chemicals. *Chem. Eng.* **2011**, *118* (2), 16−20.
(5) Yu, Z. H. et al. *Multi-burner Gasification Reactor for Gasification of Slurry or Pulverized Hydrocarbon Feed Materials and Industry Applications Thereof*. United States Patent 7,862,632 B2, Jan 4, 2011.
(6) Gong, Y.; Guo, Q. H.; Liang, Q. F.; Zhou, Z. J.; Yu, G. S. Three-Dimensional Temperature Distribution of Impinging Flames in an Opposed Multiburner Gasifier. *Ind. Eng. Chem. Res.* **2012**, *51* (22), 7828−7837.
(7) Sun, Z. H.; Dai, Z. H.; Zhou, Z. J.; Guo, Q. H.; Yu, G. S. Numerical Simulation of Industrial Opposed Multiburner Coal−Water Slurry Entrained Flow Gasifier. *Ind. Eng. Chem. Res.* **2012**, *51* (6), 2560−2569.
(8) Yu, G. S.; Yan, Z. Y.; Liang, Q. F.; Guo, Q. H.; Zhou, Z. J. The investigations of temperature distributions in an opposed multi-burner gasifier. *Energy Convers. Manage.* **2011**, *52*, 2235−2240.
(9) Karlsson, B.; Quintiere, J. G. *Enclosure fire dynamics*; CRC Press: Boca Raton, FL, 2000.
(10) Thomas, P. H.; Hinkley, P. L.; Theobald, C. R.; Simms, D. L. *Investigations into the Flow of Hot Gases in Roof Venting*; HMSO: London, U.K., 1963; Fire Research Technical Paper No. 7.
(11) Zukoski, E. E. *Properties of fire plumes, Combustion Fundamentals of Fire*; Academic Press: London, U.K., 1995.
(12) Heskestad, G. Fire Plumes. In *SFPE Handbook of Fire Protection Engineering*; Natl Fire Protection Assn: Quincy, U.S.A., 1995.
(13) Mikofski, M. A.; Williams, T. C.; Shaddix, C. R.; Blevins, L. G. Flame height measurement of laminar inverse diffusion flames. *Combust. Flame* **2006**, *146*, 63−72.
(14) Roper, F. G. The prediction of laminar jet diffusion flame sizes: Part I. Theoretical model. *Combust. Flame* **1977**, *29*, 219−226.
(15) Kiran, D. Y.; Mishra, D. P. Experimental studies of flame stability and emission characteristics of simple LPG jet diffusion flame. *Fuel* **2007**, *86*, 1545−1551.
(16) Chuah, K. H.; Kushida, G. The prediction of flame heights and flame shapes of small fire whirls. *Proc. Combust. Inst.* **2007**, *31*, 2599−2606.
(17) Lippmann, G. Epreuves reversibles, photographies integrales. *Acad. Sci.* **1908**, *146*, 446−551.
(18) Liang, C.; Lin, T.; Wong, B.; Liu, C.; Chen, H. Programmable aperture photography: multiplexed light field acquisition. *ACM. Trans. Graphic.* **2008**, *27* (3), 1−10.
(19) Adelson, E.; Wang, J. Single lens stereo with a plenoptic camera. *IEEE Trans. Pattern Anal. Machine Intell.* **1992**, *14* (2), 99−106.
(20) Levoy, M.; Ng, R.; Adams, A.; Footer, M.; Horowitz, M. Light field microscopy. *ACM Trans. Graph.* **2006**, *25* (3), 924−934.
(21) Georgeiv, T.; Intwala, C. *Light field camera design for integral view photograph*; Adobe System, Inc.: New York, 2006.
(22) Ng, R.; Levoy, M.; Bredif, M.; Duval, G.; Horowitz, M.; Hanrahan, P. *Light Field Photography with a Hand-Held Plenoptic Camera*; Stanford University: Palo Alto, CA, 2005; Computer Science Tech Report CSTR 2005-02.
(23) Perwass, C.; Wietzke, L. Single Lens 3D-Camera with Extended Depth-of-Field. *Proceedings of SPIE 8291, Human Vision and Electronic Imaging XVII*, Burlingame, CA, Jan 23−26, 2012; 829108.
(24) Bishop, T.; Favaro, P. Plenoptic depth estimation from multiple aliased views. *IEEE 12th International Conference on Computer Vision Workshops (ICCV Workshops)*, Kyoto, Japan, Sept 27−Oct 4, 2009; pp 1622−1629.
(25) Smith, W. E.; Vakil, N.; Maislin, S. A. Correction of distortion in endoscope image. *IEEE Trans. Med. Imag.* **1992**, *11*, 117−122.
(26) Hideaki, H.; Yagihashi, N. Y.; Miyake, Y. A new methed for distortion correction of electronic endoscope image. *IEEE Trans. Med. Imag.* **1995**, *14*, 548−555.
(27) Rottier, C.; Godard, G.; Corbin, F.; Boukhalfa, A. M.; Honore, D. An endoscopic particle image velocimetry system for high-temperature furnaces. *Meas. Sci. Technol.* **2010**, *21*, 115404.
(28) Wengert, C.; Reeff, M.; Cattin, P.; Szekely, G. Fully Automatic Endoscope Calibration for Intraoperative Use. *Bildverarbeitung für die Medizin, Algorithmen Systeme Anwendungen, Proceedings des Workshops* **2006**, *19* (21), 419−423.
(29) Heikkila, J.; Silven, O. A four-step camera calibration procedure with implicit image correction. *Proc. Comput. Vision Pattern Recog.* **1997**, 1106−1112.
(30) Chamberlin, D. S.; Rose, A. The flicker of luminous flames. *Ind. Eng. Chem.* **1928**, *20* (10), 1013−1016.
(31) Cetegen, B. M.; Ahmed, T. A. Experiments on the periodic instablibity of buoyant plumes and fires. *Combust. Flame* **1993**, *93*, 157−184.
(32) Pagni, P. J. Pool fire vortex shedding frequences. *Appl. Mech. Rev.* **1990**, *43*, 153−170.
(33) Darabkhani, H. G.; Bassi, J.; Huang, H. W.; Zhang, Y. Fuel effects on diffusion flames at elevated pressures. *Fuel* **2009**, *88*, 264−271.
(34) Chen, Z. B.; Hu, L. H.; Huo, R.; Zhu, S. Flame Oscillation Frequency Based on Image Correlation. *J. Combust. Sci. Technol.* **2008**, *14* (4), 367−671 In Chinese..
(35) Liao, B.; Chen, Y. An image quality assessment algorithm based on dual-scale edge structure similarity. Presented at the *Second International Conference on Innovative Computing, Information and Control*, Kumamoto, Japan, Sep 5−7, 2007.